

Electronic supplementary information

1. Molecular Structures of complexes studied

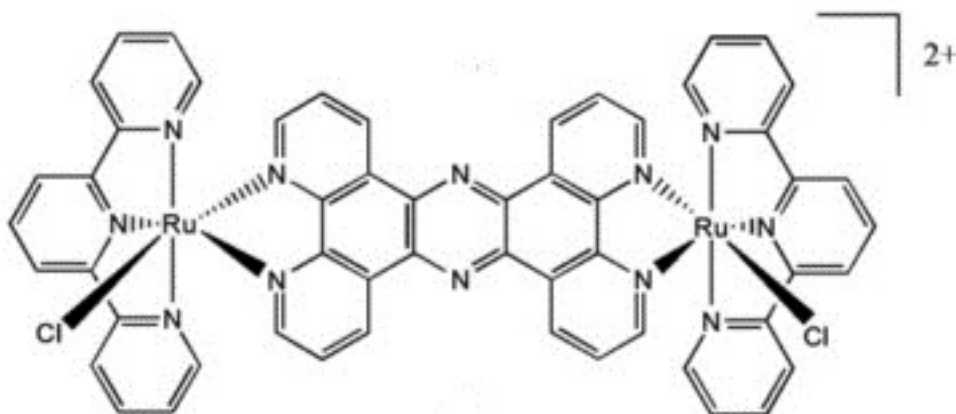


Figure S1: Molecular structure of [Cl(2,2' ;6' ,2''-terpyridine)Ru(tetrapyrido[3,2- α :2' ,3' - c:3'' ,2''-h:2'' ,3''-j]phenazine)Ru(2,2' ;6' ,2''-terpyridine)Cl](PF₆)₂ (+2Ru₂)

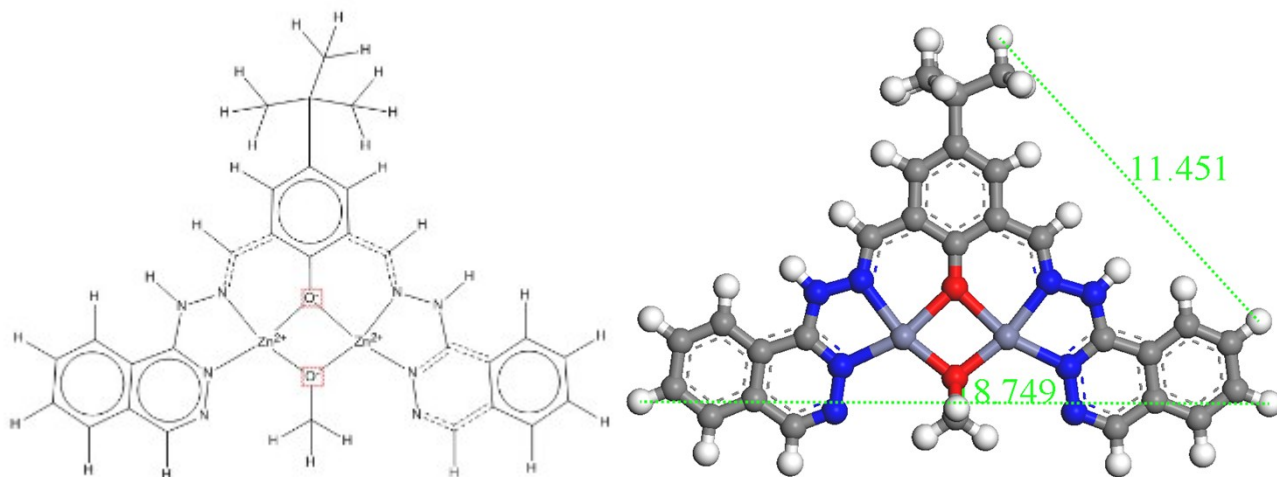


Figure S2A: Molecular structure and DFT Geometry Optimized structure of 4-(tert-butyl)-2,6-bis((2-(phthalazin-1-yl)hydrazono)methyl)phenol (m₂-methoxo) dizinc(II)-acetate (+2Zn₂)

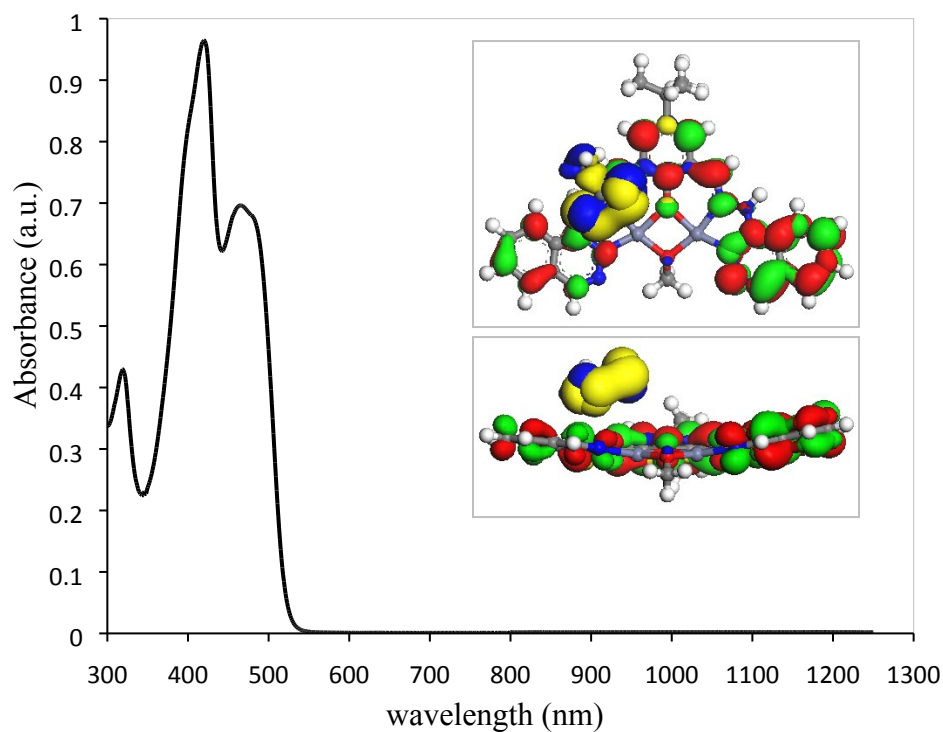


Figure S3A: UV-Vis-NIR spectra of **+2Zn2** in dry DMF. Molar extinction $\epsilon_{420} = 38700 \pm 400 \text{ M}^{-1} \text{ cm}^{-1}$ (value \pm standard error, 95%) at $\lambda = 420 \text{ nm}$ was determined by method of dilutions. Absorbance versus concentration was linear from $0.1 \mu\text{M}$ to $10 \mu\text{M}$. No evidence of complex dimerization was observed. DFT calculations of frontier molecular orbitals (inset). Absorptions at 420 nm and at 480 nm are due to ion-pair $\rightarrow \pi^*$ charge transfer transitions. The absorption at 320 nm is consistent with the ligand's $\pi \rightarrow \pi^*$ transition.

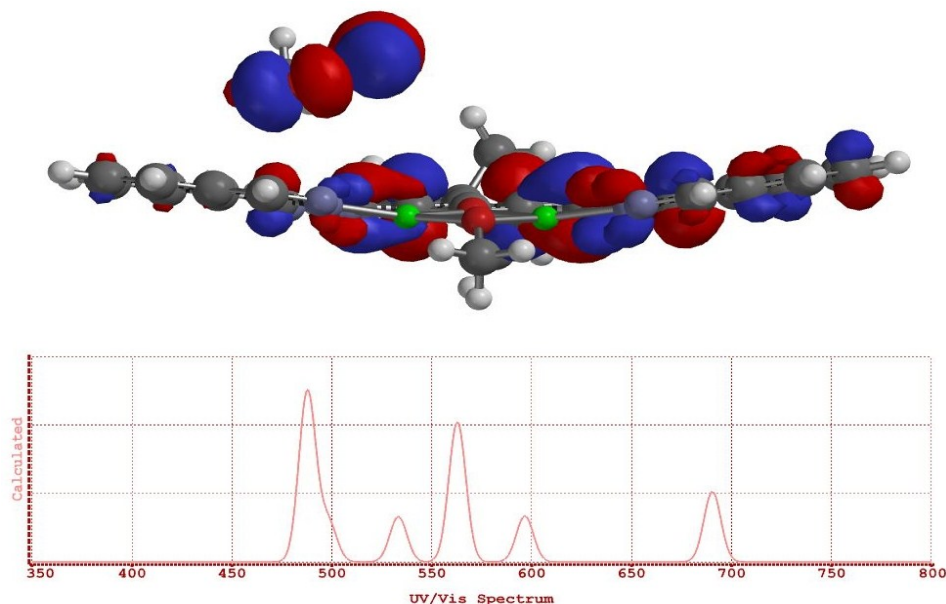


Figure S3B: TD-DFT calculation (Spartan 10, B3LYP in DMF) of the $[+2Zn_2](Ac)$ complex in DMF ion-pairing with one acetate. HOMO resides completely on the acetate and LUMO resides on the hydrazine ligand. Calculate UV-Vis spectra is consistent with experimental spectra. Calculated transitions are at 488, 498, 533, 562, 596, and 690 nm and appear redshifted by ~ 160 nm compared to experimental transitions from spectra in S3A. The transition at 320 nm is consistent with the ligand's $\pi \rightarrow \pi^*$ transition. This is not a computational paper and we do not seek or claim accuracy in the DT results other than to support an ion-pair model as expected from ILCT transitions shown here.

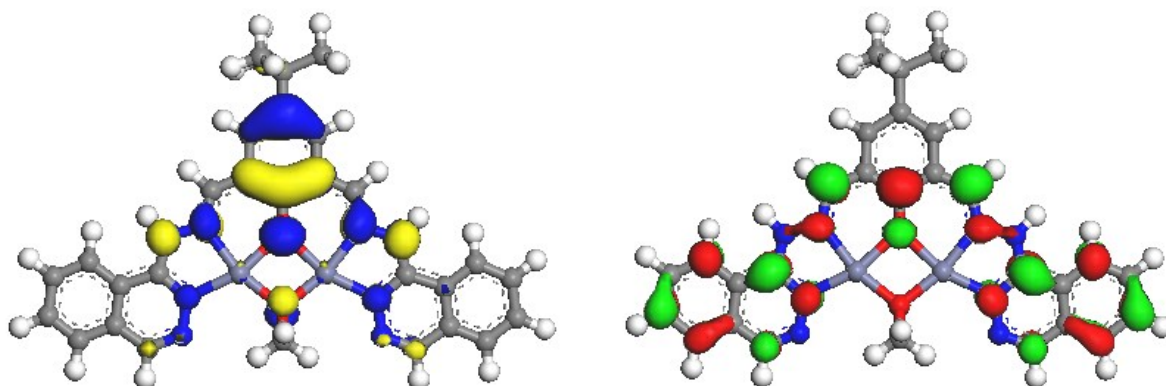


Figure S3C: DFT calculation of the $+2\text{Zn}2$ complex in DMF without any ion-pairing. HOMO (blue-yellow) left and LUMO (green-red) right both reside on the ligand. No orbital density on the metal centers for the frontier orbitals or HOMO-1, or HOMO-2. No indication of MLCT adsorption capabilities.

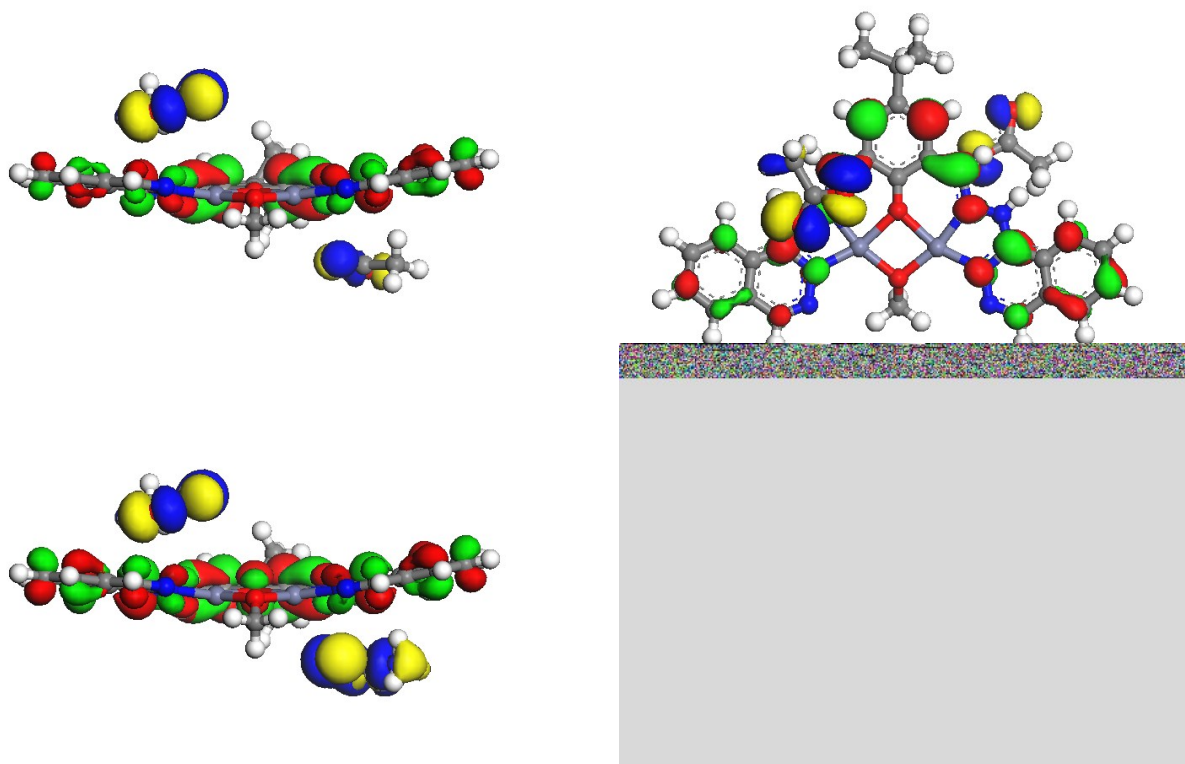


Figure S3D: DFT calculation of the $[\text{+}2\text{Zn}2](\text{Ac})_2$ complex in DMF showing the neutral species from ion-pairing. HOMO (blue-yellow) and LUMO (green-red), edge view left, plan view right. No orbital density on metal centers (Zn atoms in grey). Bottom row is the same as the top row but includes all orbitals from HOMO-2 through LUMO+2.

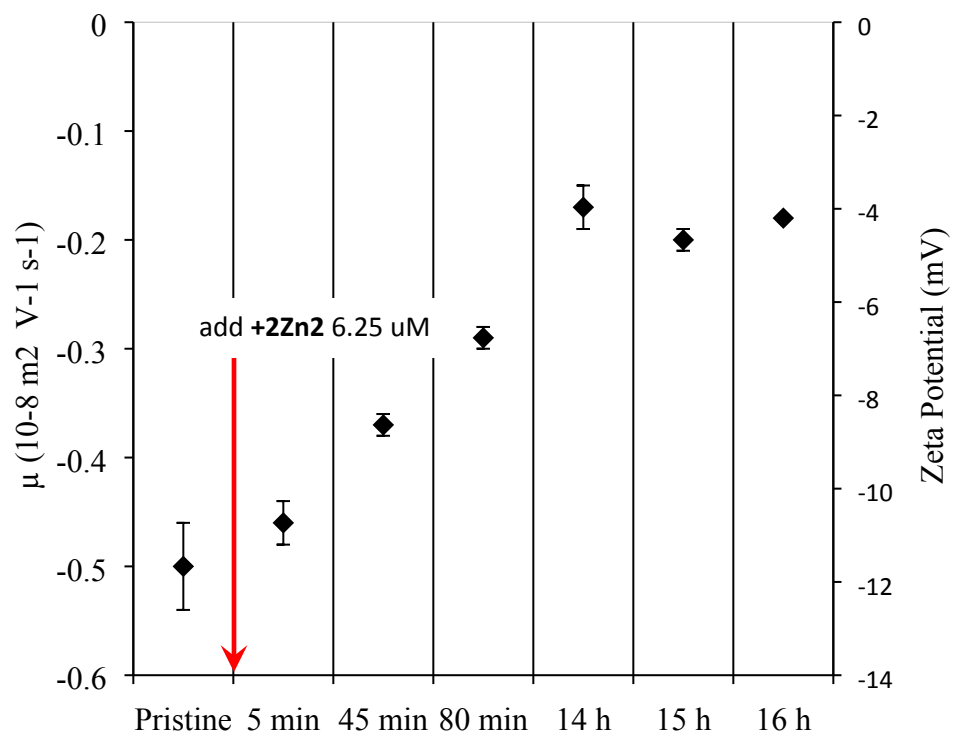


Figure S4: Electrophoretic mobility and zeta potential of SWCNTs in DMF before and after **+2Zn2** is added. T= 25 °C

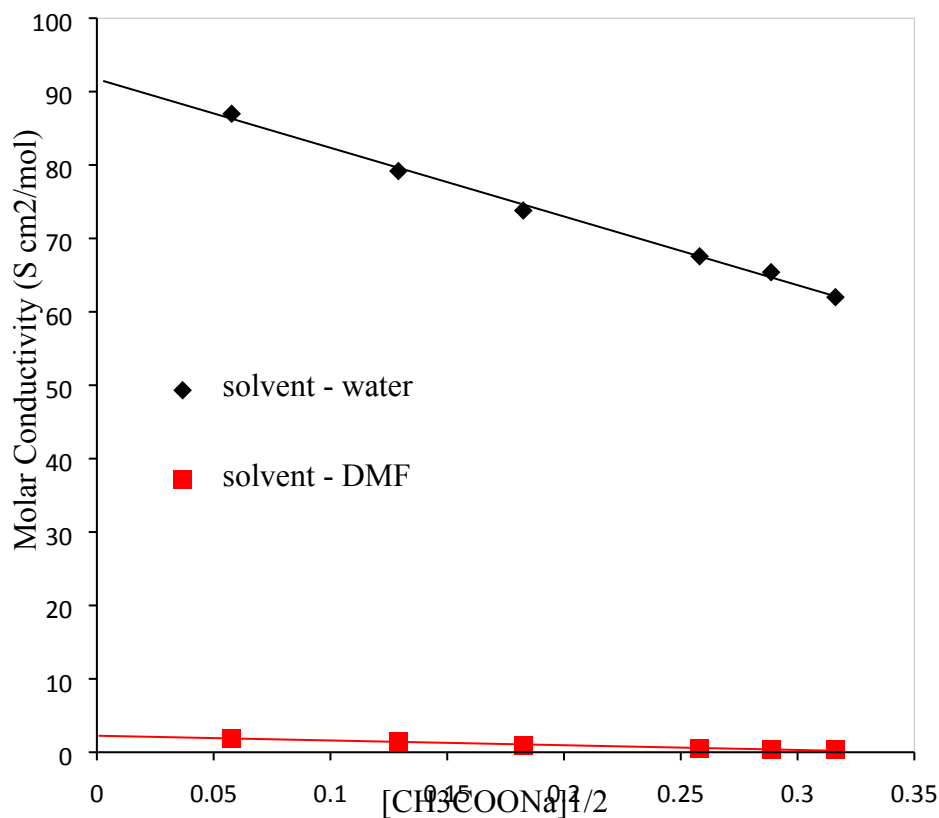


Figure S5: Limiting molar conductivity Λ_m^0 of sodium acetate as determined by the y-intercept using Kohlrausch's law: $\Lambda_m = \Lambda_m^0 - K[NaAc]^{1/2}$. The limiting molar conductivity for sodium acetate in DMF is $\Lambda_0 = 2.4 \pm 0.1 \text{ S cm}^2 \text{ mol}^{-1}$ (data shown in red) whereas the salt is fully dissociated in water with $\Lambda_0 = 92.7 \pm 0.7 \text{ S cm}^2 \text{ mol}^{-1}$ (data shown in black).

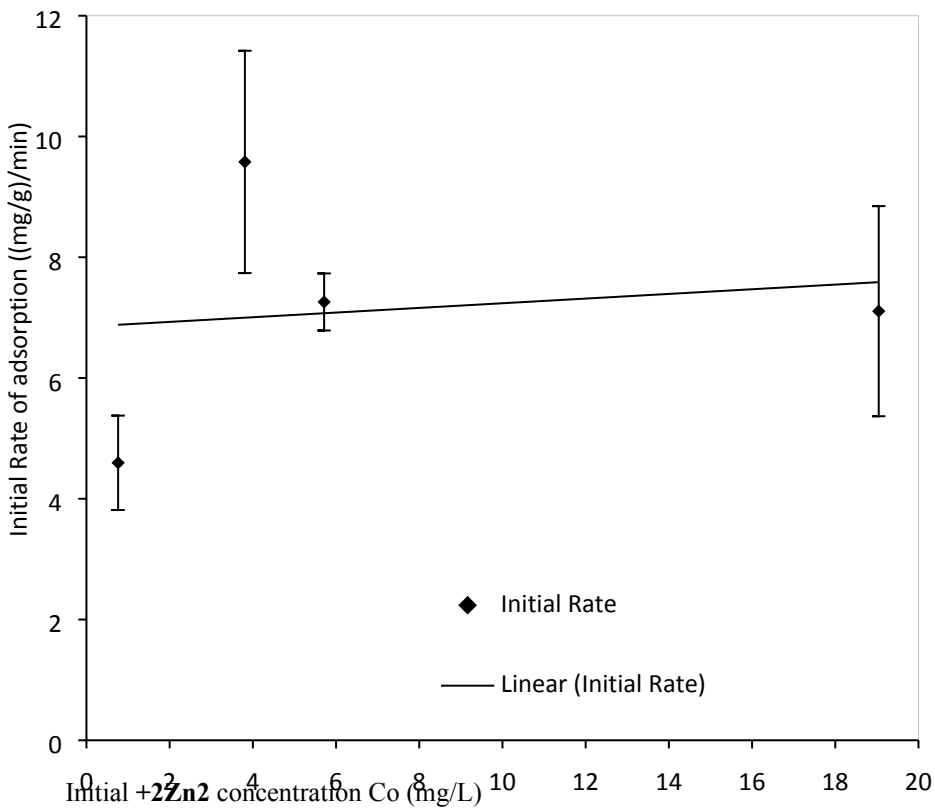


Figure S6: Initial Rate of adsorption versus initial concentration of Zn^{2+} . Initial rate is independent of C_o especially at higher initial concentrations where the experiment is easier and more reproducible.

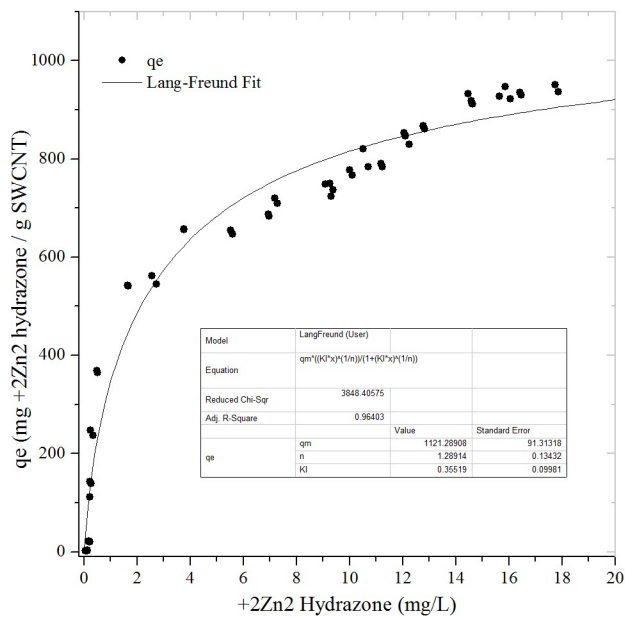
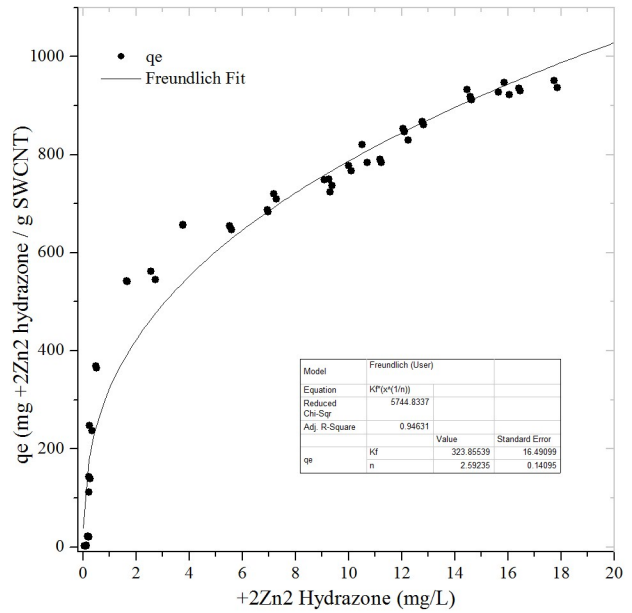
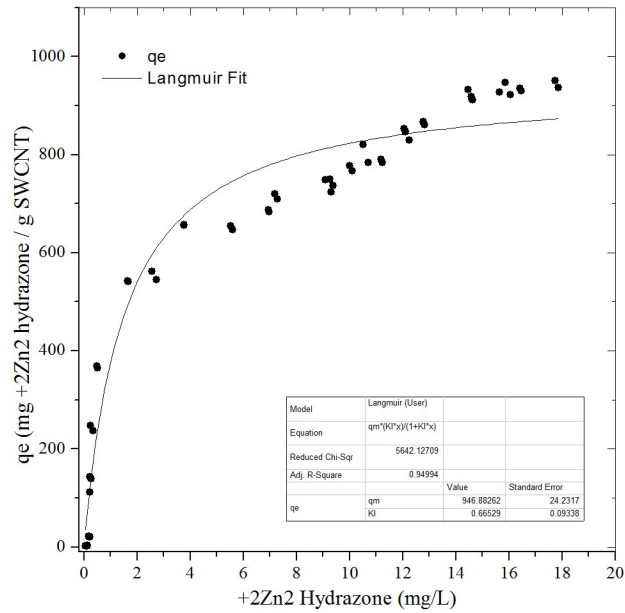


Figure S7A-C: The same adsorption isotherm data as in Fig 4 but fit with a Langmuir (A), Freundlich (B), and 3-parameter Langmuir-Freundlich (C) models. The BET model in Fig. 4 is the best fit.

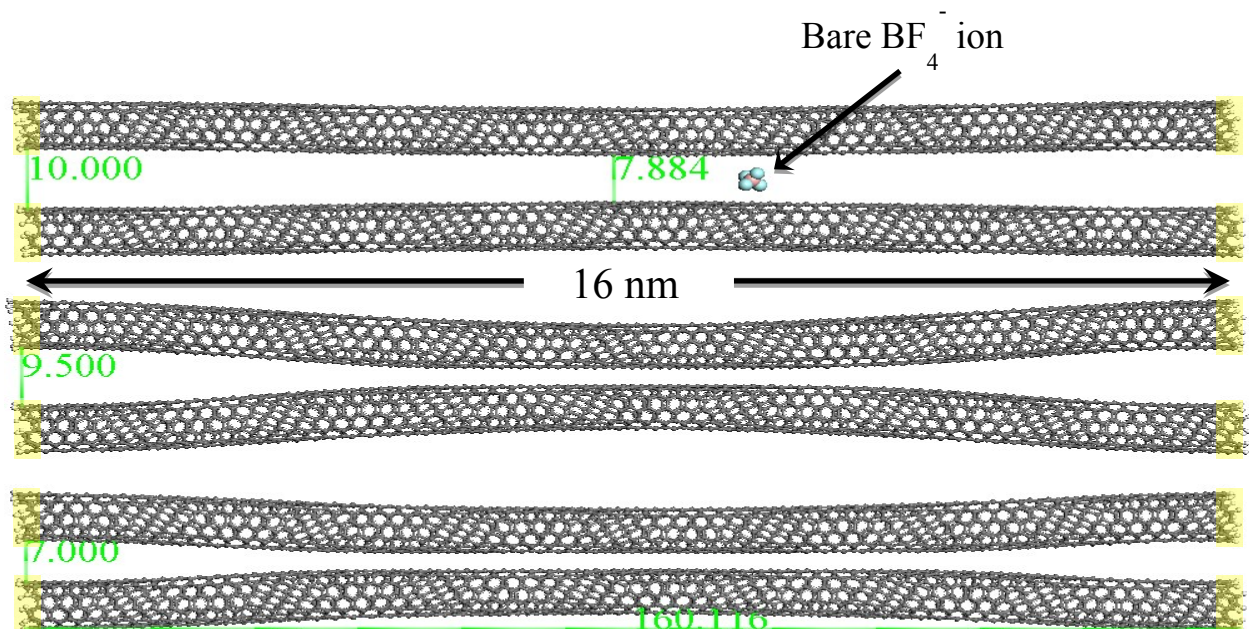


Figure S8: Molecular mechanics geometry optimization, using the COMPASS force field and a dielectric contact of 36.7 to simulate DMF solvent, of pair of SWCNTs interacting through DMF while being separated at their ends by molecular spacers. As the spacers are moved farther apart axial the SWCNTs collapse due to vdW attractive forces. As the molecular spacers become more sterically bulky, the ends of the tubes stay farther apart leading to a stable mechanical system. The SWCNT pair at top has an intertube spacing of 0.79 nm which is enough room for fast ion access to the EDL surface area.

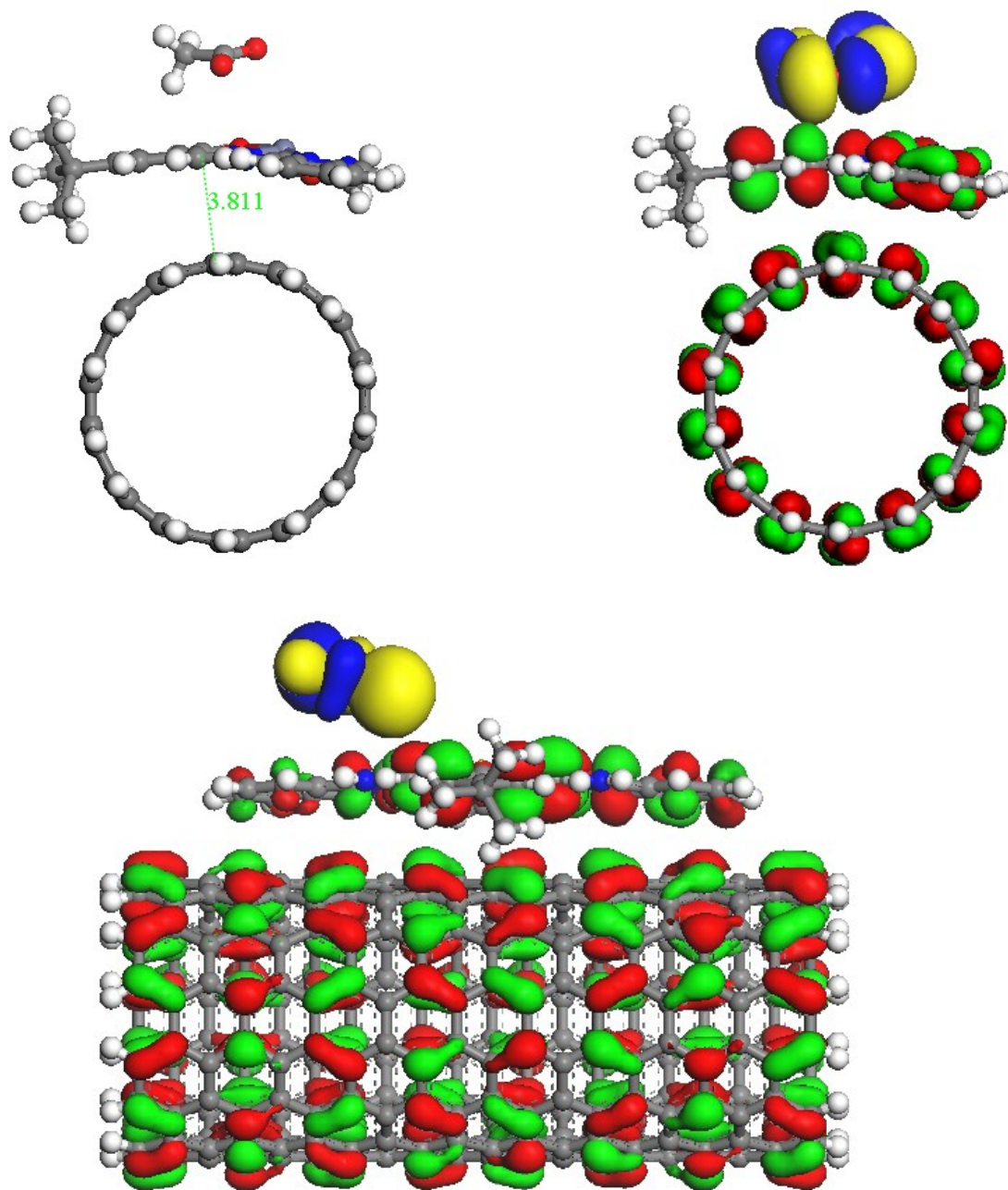


Figure S9A: DFT geometry optimization of the ion-complex-SWCNT cluster in DMF. The HOMO-2 resides on the acetate (blue-yellow) and the LUMO+2 resides on the hydrazone ligand and the SWCNT (green-red) (upper-right looking down the SWCNT). Lower panel is the same as upper right looking perpendicular to the SWCNT.

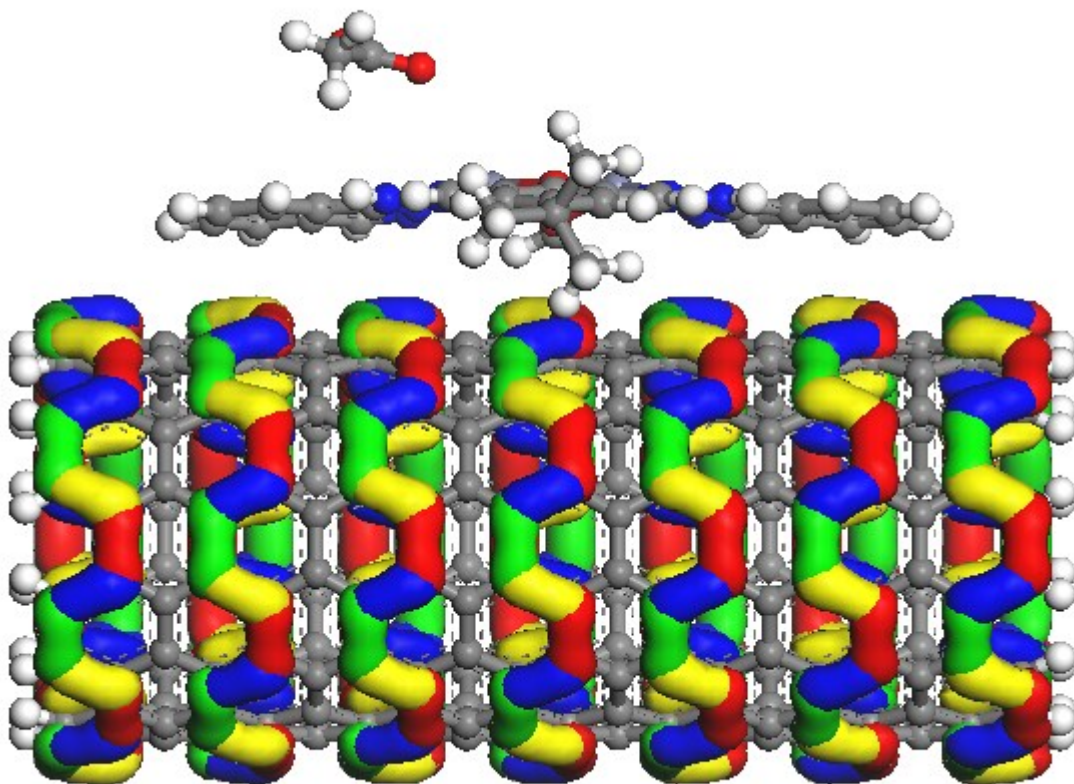


Figure S9B: DFT geometry optimization of the ion-complex-SWCNT cluster in DMF showing the HOMO (blue-yellow) and LUMO (green-red) residing completely on the SWCNT. These data suggest that electron density can easily be transferred between the SWCNTs and the hydrazine ligands. This can result in additional fast faradaic pseudo-capacitance for use as an electrical energy storage material